Microwave-assisted optimization of the manganese redox states for enhanced capacity and capacity retention of $LiAl_xMn_{2-x}O_4$ (x = 0 and 0.3) spinel materials

Funeka P. Nkosi[1,2], Charl J. Jafta[2], Mesfin Kebede[2], Lukas le Roux[2], Mkhulu K. Mathe[2], and Kenneth I. Ozoemena[*,1,2]

[1.] *Department of Chemistry, University of Pretoria, Pretoria 0002, South Africa.*

[2.] *Energy Materials, Materials Science and Manufacturing, Council for Scientific & Industrial Research (CSIR), Pretoria 0001, South Africa*

A manuscript to be submitted to *RSC Advances*

[*]Author to whom correspondence should be addressed: (K.I. Ozoemena): Tel.:+27128413664; Fax: +27128412135; E-mail: kozoemena@csir.co.za

Abstract

Microwave irradiation at the pre- and post-annealing steps of the synthesis of $LiAl_xMn_{2-x}O_4$ (x = 0 and 0.3) spinel cathode materials for rechargeable lithium ion battery is a useful strategy to optimize the average manganese valence number (n_{Mn}) for enhanced capacity and capacity retention. The strategy impacts on the lattice parameter, average manganese valence, particle size and morphology, reversibility of the de-intercalation/intercalation processes, and capacity retention upon continuous cycling. Microwave irradiation is able to shrink the particles for improved crystallinity. The XPS data clearly suggest that microwave irradiation can be used to tune the manganese valence (n_{Mn}), and that the $LiAl_xMn_{2-x}O_4$ with $n_{Mn} \approx 3.5+$ gives the best electrochemical performance. These new findings promise to revolutionize how we use microwave irradiation in the preparation of energy materials and various other materials for energy storage and conversion materials for enhanced performance.

Keywords: Microwave; Lithium manganese oxide; manganese valence number; capacity retention.

Introduction

Rechargeable lithium ion batteries (RLIBs) have proved themselves as the most attractive advanced battery technologies for electric vehicles and portable electronics.[1-8] Perhaps, the lithium manganese oxide, $LiMn_2O_4$ (LMO) spinel material needs little or no introduction as it has proved itself as one of the most attractive cathode material for RLIBs due to its high operating voltage (4 V), low cost, environmental compatibility, and stability at low temperature compared to other cathode materials.[5, 9-11] LMO has begun to show some commercial success; it is the cathode material that drives Nissan Leaf (a pure electric vehicle) and Chevrolet Volt (a plug-in hybrid electric vehicle). Despite the advantages of LMO, one of its major challenges that still conspire against its full utilization is capacity fading upon continuous cycling. The capacity loss is caused by two main factors, the so-called Jahn-Teller distortion and slow dissolution of manganese in the electrolyte.[12, 13] The Jahn-Teller effect is the reduction of the crystal symmetry from cubic to tetragonal structure, and it is this structural transition that deteriorates its cycle life and is said to occur when the average manganese valence number (n_{Mn}) is equal or less than 3.5.[14, 15] The stress generated by this phenomenon leads to cracking of particles and loss of electric contact upon cycling. The manganese ions in LMO are believed to exist as 50% Mn^{3+} and 50% Mn^{4+} (i.e., n_{Mn} = 3.5+). High content of Mn^{3+} ions causes capacity fading, and leads to the dissolution of the cathode material into the electrolyte.

There are three known strategies for improving the cycling performance of LMO; (i) making the spinel structure lithium-rich (Li-excess),[16-18] (ii) doping with cations[19-21] and (iii) coating with metal oxides. Aluminium is a preferred dopant for LMO[16-18] since it is abundant, non-toxic, less expensive and lighter than transition metal elements. Reports on the application of microwave irradiation (MWI) in the preparation of LMO have focussed on

reducing the synthesis time,[22-28] there is no report on the strategic utilisation of MWI aimed at curbing the recalcitrant capacity fading. We have found that microwave irradiation can enhance cycling behaviour by controlling the manganese valence state, structure, and morphological integrity of the LMO and Al-doped LMO. In a nutshell, the MWI is a viable 'curative' treatment to LMO powder to enhance its capacity retention.

Experimental procedure

Chemicals and materials

Lithium nitrate ($LiNO_3$), manganese nitrate tetrahydrate ($Mn(NO_3)_2{\cdot}4H_2O$), Urea ($CO(NH_2)_2$) and aluminium nitrate nonahydrate ($Al(NO_3)_2{\cdot}9H_2O$), were used for the preparation of the cathode materials.. Carbon black, N-methyl-2-pyrrolidone (NMP) and polyvinylidene fluoride (PVDF) were used to make the paste. Aluminium foil (MTI corporation USA, 50 μm thick), lithium metal (Sigma-Aldrich,50 μm thick), lithium hexafluorophosphate ($LiPF_6$), ethylene carbonate (EC), diethyl carbonate (DEC) and dimethyl carbonate (DMC) were used during the fabrication of the coin cells. All the chemicals were purchased from Sigma-Aldrich and used without further purification.

Synthesis of LMO and Al-doped LMO powders

A combustion method was used to synthesize spinel LMO-based powders directly from lithium nitrate, manganese nitrate and urea. $LiNO_3$ (1.10 g, 0.016 mol.), $Mn(NO_3)_2{\cdot}4H_2O$ (8.00 g, 0.032 mol.) and urea (2.87 g, 0.047 mol.) were dissolved in deionised water (20.00 ml) and stirred until the starting materials were completely dissolved. The resultant solution was heated in the furnace at 550 °C for ~7 min to yield a black powder product. The powders were ground using pestle and mortar prior to the heat treatments below. To study the influence of microwave irradiation, two batches of the powders were synthesised. These

powders were subjected to microwave irradiation (using the Anton Paar Multiwave 3000 system, $\lambda = 0.12236$ m) at 600 W for 20 min prior to or post-annealing as may be required. The sample powders were annealed at 700°C for 10 h using a tube furnace (50 mm, MTI Corporation). The resulting powders were lithium manganese oxide-microwaved and then annealed (LMO-ma) and lithium manganese oxide–annealed and then microwaved (LMO-am). The LMO powder sample that was obtained by the conventional annealing at 700°C for 10 h is abbreviated herein as LMO-a. The aluminum-doped LMO ($LiMn_{1.7}Al_{0.3}O_4$) were prepared using the same procedure as for the LMO-based samples. The $LiMn_{1.7}Al_{0.3}O_4$ powders were prepared using 1.10 g $LiNO_3$, 6.80 g $Mn(NO_3)_2{\cdot}4H_2O$, 1.80 g $Al(NO_3)_2{\cdot}9H_2O$) and 2.87 g Urea. The powders were similarly named LMOA-a, LMOA-am and LMOA-ma. The schematic of the procedure is summarized in **Fig. 1**.

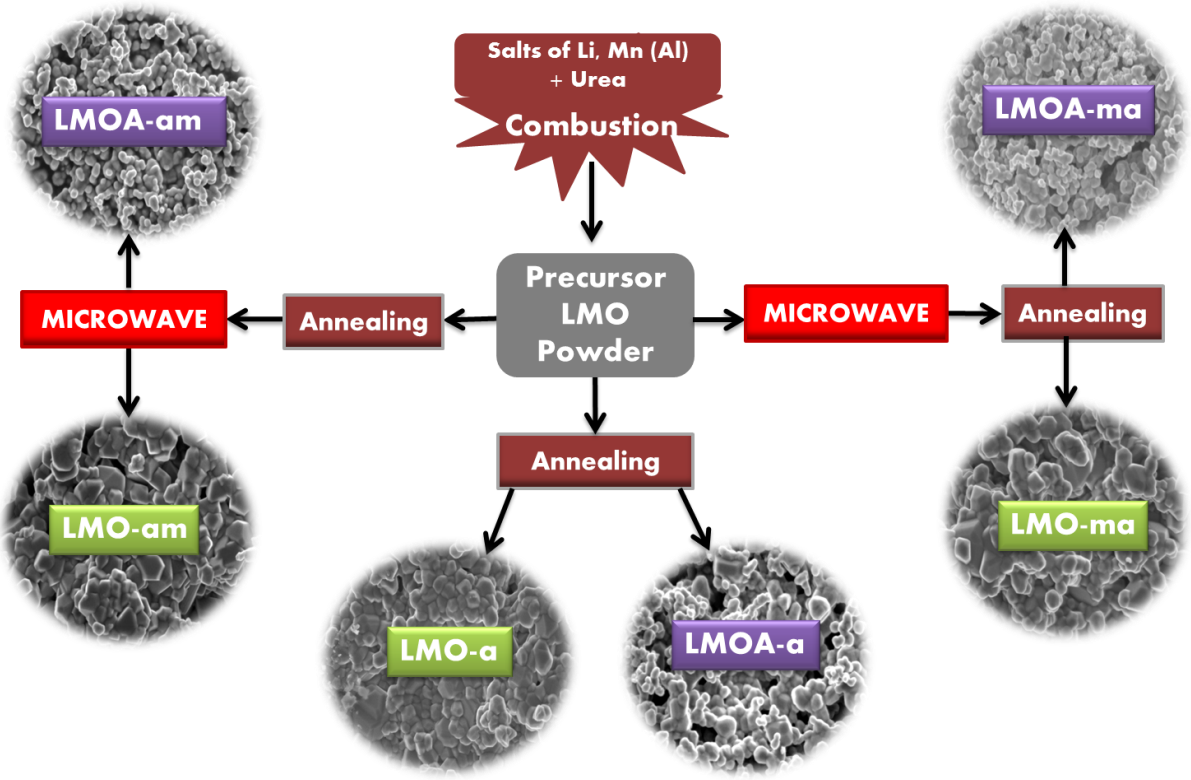

Fig. 1: Schematic representation of the microwave-assisted combustion synthesis of $LiMn_2O_4$ (LMO) and $LiMn_{1.7}Al_{0.3}O_4$ (LMOA). The abbreviations are as described in the experimental section.

Materials characterization

Scanning electron microscopic micrographs were acquired using a LEO 1525 field emission scanning microscope (FE-SEM) with the acceleration voltage of 200 kV. HRTEM measurements were carried out on a Joel HRJEM-2100 microscopy using LAB6 filament as an electron source. The measurements were carried out using electron beam at 200kV. Powder XRD data were acquired using a PANalytical X'Pert Pro diffractometer with CuKα

radiation, λ=1.5046A as a radiation source operating at 45 kV and 40 mA, scan range between 0 and 90°. XPS measurements were carried out using Kratos Axis Ultra-DLD system (Shimadzu) with Al Kα radiation (1486.6 eV). The binding energy was calibrated with reference to the C 1s level of the carbon (284.6 eV). The FTIR spectra were recorded using a Perkin Elmer Spectrum 100 FTIR spectrometer in the range 400-4000 cm^{-1}. The analysis was carried out using a diamond crystal probe and air was used as a background. Pellets of the samples were mixed with KBr in the ratio 1:3 and prepared by the disk method. The pellets were made using a thickness that provided good transparency for IR radiation. Raman measurements were carried out in air using a Horiba Jobin Yvon spectrometer equipped with 10x objective lens to focus the laser beam on a small selected area of the sample, a 30 mW green argon laser (λ = 514 nm) an excitation source, and a 1800 lines/mm grating monochromator with an air-cooled CCD detector. Raman spectra were measured up to 1000 cm^{-1} on the stokes side, with a spectral resolution of about 3 cm^{-1}.

Fabrication of coin cells and electrochemical characterization

The cathodes for the electrochemical studies were prepared by making up of slurry which contained 80% of the LMO powders mixed with 10% carbon black and 10% polyvinylidene fluoride (PVDF) binder in N-methyl-2-pyrrolidone (NMP) as the solvent. The slurry was applied using a doctor-blade method onto an aluminium foil as a current corrector. The coated aluminium foil was dried under vacuum at 110 ^{o}C for 12 h, then pressed to form a uniform layer. The electrodes were heated at 80 ^{o}C under vacuum for at least 6 h, and then kept in the glovebox (MBRAUN MB10 compact) for 2 h before the fabrication of the coin cells. The coin cells (type CR 2032) composed of the positive electrode (cathode) made from the required spinel LMO powder, lithium metal as the negative electrode (anode) and a

Celgard polypropylene-based membrane separator soaked in non-aqueous electrolyte. A 1 M $LiPF_6$ in EC/DC/DMC in 1:1:1 volume ratio solution was used as the electrolyte. $LiPF_6$ in EC-DMC-DEC has increased ion mobility and high ionic conductivity compared to a commercial electrolyte with $LiPF_6$ in EC/DEC. High conductivity of the electrolyte will minimize the internal resistance of the cell.

The coin cells also contained a stainless steel spacer to provide an electrical connection from the electrode to the case, and a spring to exert pressure on the components to allow maximum contact of the cathode and anode when the coin cell is sealed. The coin cells were assembled in a glovebox filled with ultra-high purity argon gas with the concentration of H_2O and O_2 maintained at < 0.5 ppm. The electrolyte was left in the glove box overnight before being used to fabricate the coin cells. After all components of the coin cells were aligned, the coin cell was sealed with a Compact Hydraulic Crimping Machine (MSK-110). The pressure on the crimper was set at 750 psi to seal the coin cells. After fabrication, the coin cells were allowed to stand for 24 h before the electrochemical measurements were performed. Cyclic voltammetry (CV) was conducted at a scan rate of 0.1 mV s^{-1} over a range of 3.5 – 4.3 V using a Bio-Logic science VMP3-based instrument using the EC-lab V10.32 software. The charge-discharge capacity and cycle performance (rate capability) were measured at different C-rates (charge-discharge rates) between 3.5 – 4.3 V using a Maccor 4000 battery tester. All of the electrochemical performance measurements were carried at room temperature.

Results and discussion

Morphological and structural characterization

The FESEM images of the spinel materials at low magnification are shown in **Fig. 2** (also see *Supporting Information, **Fig. S1*** for high magnification). The LMOA samples are smaller in size (10 – 130 nm) than the LMO samples (80 – 250 nm) or the commercial LMO sample (LMO-comm, ≥ 1 μm, *Supporting Information*, ***Fig. S2***). From the comparative TEM images of the LMO-based samples (**Fig. 3**) and the LMOA-based samples (*Supporting Information*, ***Fig. S3***), the spinels are crystalline, with well-defined lattice fringes, and an average d-spacing of 0.473±0.04 nm which confirm the (111) plane in the lattice structure.

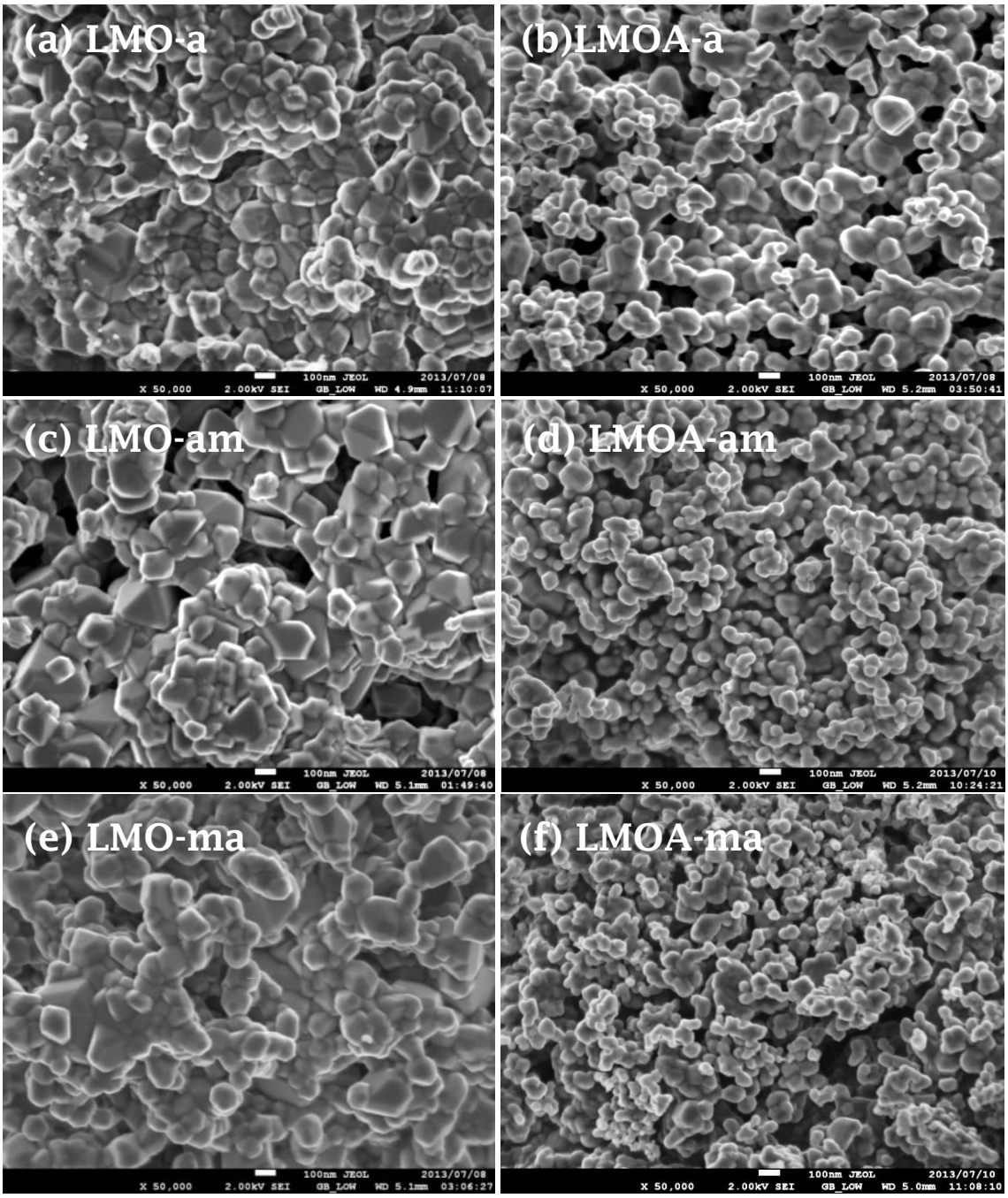

Fig. 2: Typical FE-SEM micrographs of LMO powders at low magnifications (100 nm). The abbreviations are as described in scheme 1.

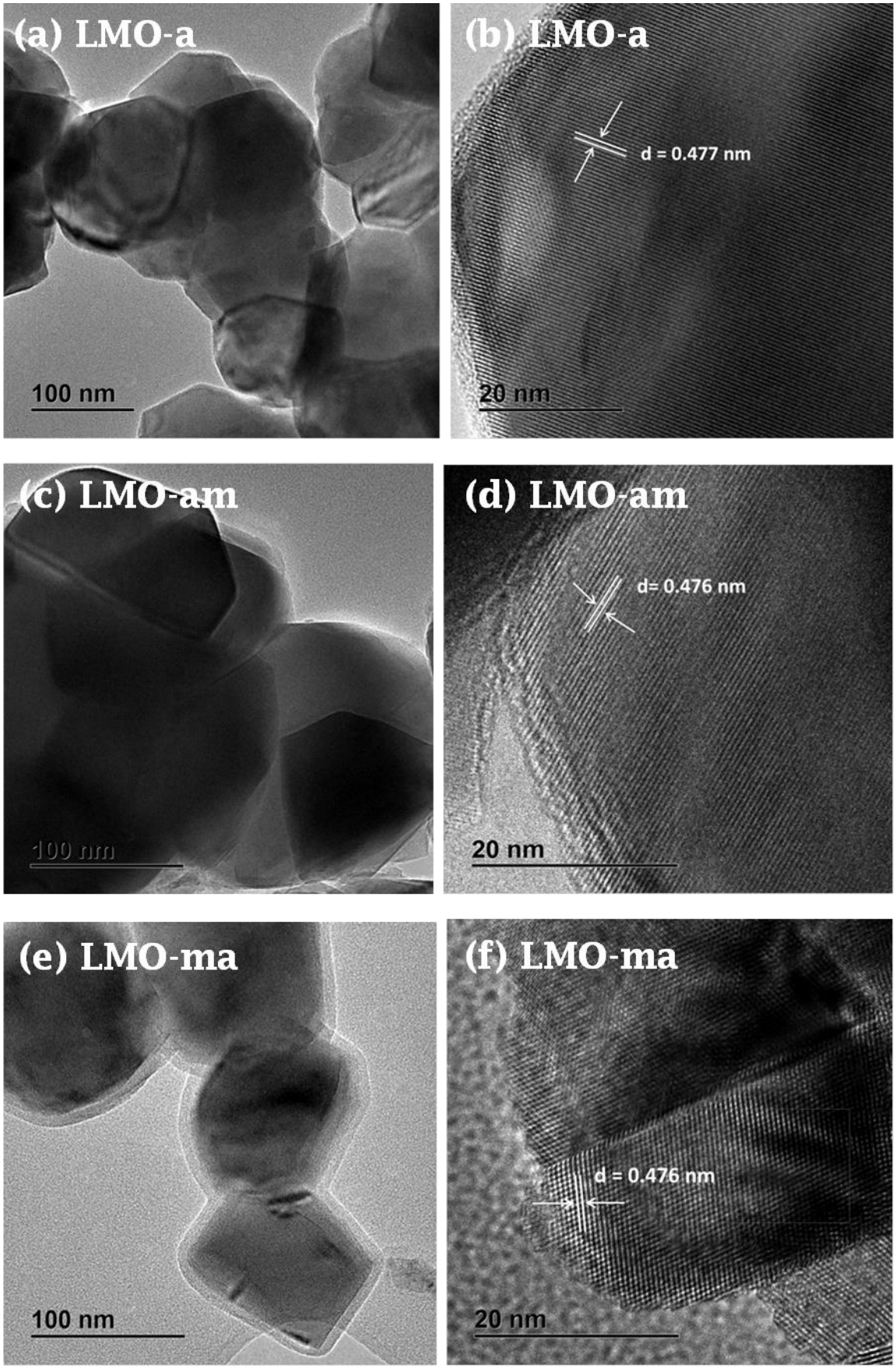

Fig. 3: Typical TEM and HRTEM images of LMO-based powders.

The powder XRD patterns for the LMO and LMOA (**Fig. 4**) showed well-developed diffraction peaks of pure spinel $LiMn_2O_4$ and $LiAl_{0.3}Mn_{1.7}O_4$ materials. The peaks were indexed to the characteristic diffractions of spinel $LiMn_2O_4$ (JCPDS File No. 88-1749) with space group *Fd*-3*m* , corresponding to the (111), (311), (222), (400), (331), (551), (440), and (531) planes. The XRD patterns are similar but the relative intensities for LMO-ma are much stronger than others, confirming the high crystalline structure for the LMO-ma, as also shown by its HRTEM image [29-31]. The lattice parameter values were determined by Rietveld analysis using the Expo2013 software. **Table 1** summarises the values of the lattice parameter with some interesting information. First, the LMO-a shows the largest lattice parameter, which decreased upon microwave irradiation and/or doping with aluminium. The lattice contraction means a decrease in the Mn^{3+} and increase in the Mn^{4+} ion (since the radius of Mn^{3+} (0.66 Å) is greater than that of Mn^{4+} (0.60 Å).[32] Second, there is a dramatic contraction of the lattice parameters for the LMOA samples which is due to the fact that the radius of Mn^{3+} is greater than that of Al^{3+} (0.53 Å), and the bond length of Mn–O (1.90 Å) is longer than that of Al–O (1.62 Å); as Al^{3+} substitutes Mn^{3+} in the 16d site of spinel structure, the unit cell shrinks. In general, the lattice contraction increases the structural stability of the spinel, which is beneficial to the suppression of Jahn–Teller distortion. The smaller intensity ratios of the (311)/(400) peaks (I_{311}/I_{400}), confirm that the two microwaved samples (LMO-ma and LMOA-am) are more crystalline than others [33, 34].

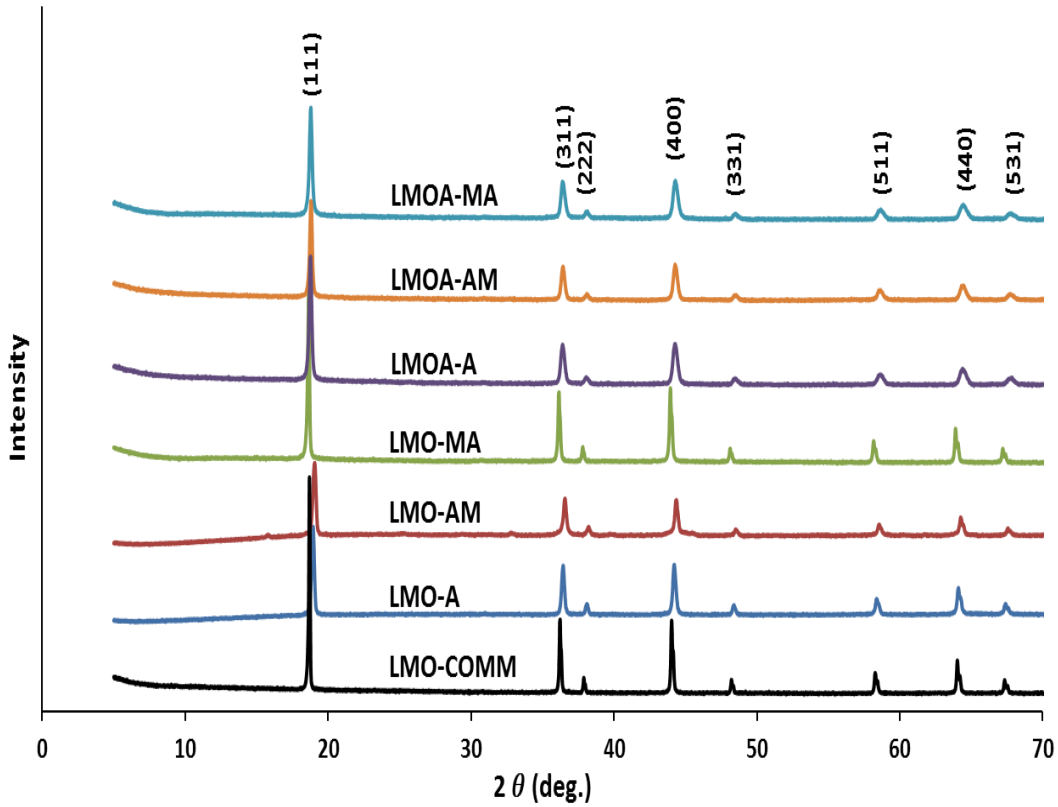

Fig. 4: Typical powder XRD patterns of the LMO- and LMOA-based powders.

Table 1: *XRD, XPS (Mn-2$p_{3/2}$ spectra) and electrochemical data of the LMO and LMOA based samples*

Sample	**XRD data**		**Binding energy position (eV)**		**Cation distribution**			**Coin cell data**	
	Lattice parameter $\pm$ 3x^{-4} (Å)	**I_{311}/I_{400}**	**Mn^{4+}**	**Mn^{3+}**	**Mn^{4+} (%)**	**Mn^{3+} (%)**	**Mn valence (n_{Mn})**	**Initial capacity (mAhg^{-1})**	**Capacity loss after 50 cycles**
LMO-a	8.2565	0.991	644.5	642.2	16.5	83.5	3.165	127.5	22.0 %
LMO-am	8.2441	1.043	645.8	642.7	49.7	50.3	3.498	94.3	9.0 %
LMO-ma	8.2403	0.944	646.5	644.6	54.2	45.8	3.541	131.5	5.0 %
LMO-comm	8.2161	1.012	644.1	642.6	40.1	59.9	3.400	-	-
LMO [35]	8.2404	1.108	-	-	51	49	3.503	118.6	66.8 %
LMOA-a	8.1701	0.991	644.4	642.4	31.0	69.0	3.310	95.3	7.2 %
LMOA-am	8.1671	0.953	644.5	642.8	49.2	50.8	3.493	103.6	0.4 %
LMOA-ma	8.1696	0.996	644.3	642.6	31.2	68.8	3.312	73.6	0.7 %

XPS is a well-known surface-sensitive technique for the quantification of cations in oxide materials including spinels.[36-44] From the Mn 2$p_{3/2}$ spectra of the spinel materials (**Fig. 4)**, the Mn^{3+}/Mn^{4+} ratio and valence number (**Table 1)** corroborate the lattice contraction observed in the XRD. The stoichiometry of all the LMO samples is the same and so as for all LMOA samples. Interestingly, the increased valence states for LMO-ma (n_{Mn} = 3.541+) and LMOA-am (n_{Mn} = 3.493+) are consistent with the slight positive shifts of their Mn-2$p_{3/2}$ binding energies compared to un-microwaved samples. Note that the n_{Mn} values for LMO-a and LMO-comm are less than 3.5+, contradicting the general notion that LMO powders should be $n_{Mn} \approx$ 3.5+.Perhaps, more interesting is that when the LMO-a was subjected to microwave irradiation to obtain the LMO-am, we observed a lattice shrinkage (from 8.256 to 8.244 Å) leading to $n_{Mn} \approx$ 3.5+. This result strongly proves that our microwave irradiation strategy is able to convert excess Mn^{3+} to Mn^{4+} to generate the expected $n_{Mn} \approx$ 3.5+ value.

The microwave-treated samples with $n_{Mn} \approx 3.5+$ (LMO-ma and LMOA-am) exhibited the strongest Raman and IR peaks (*Supporting Information*, ***Fig. S4***), confirming the effect of the microwave irradiation in strengthening the Mn-O bonding for enhanced electrochemistry. The LMOA samples showed positive peak shifts (≥ 20 cm^{-1}), which indicates a relatively stronger bonding in the $Mn(Al)O_6$ octahedra due to Al-doping and the microwave irradiation.

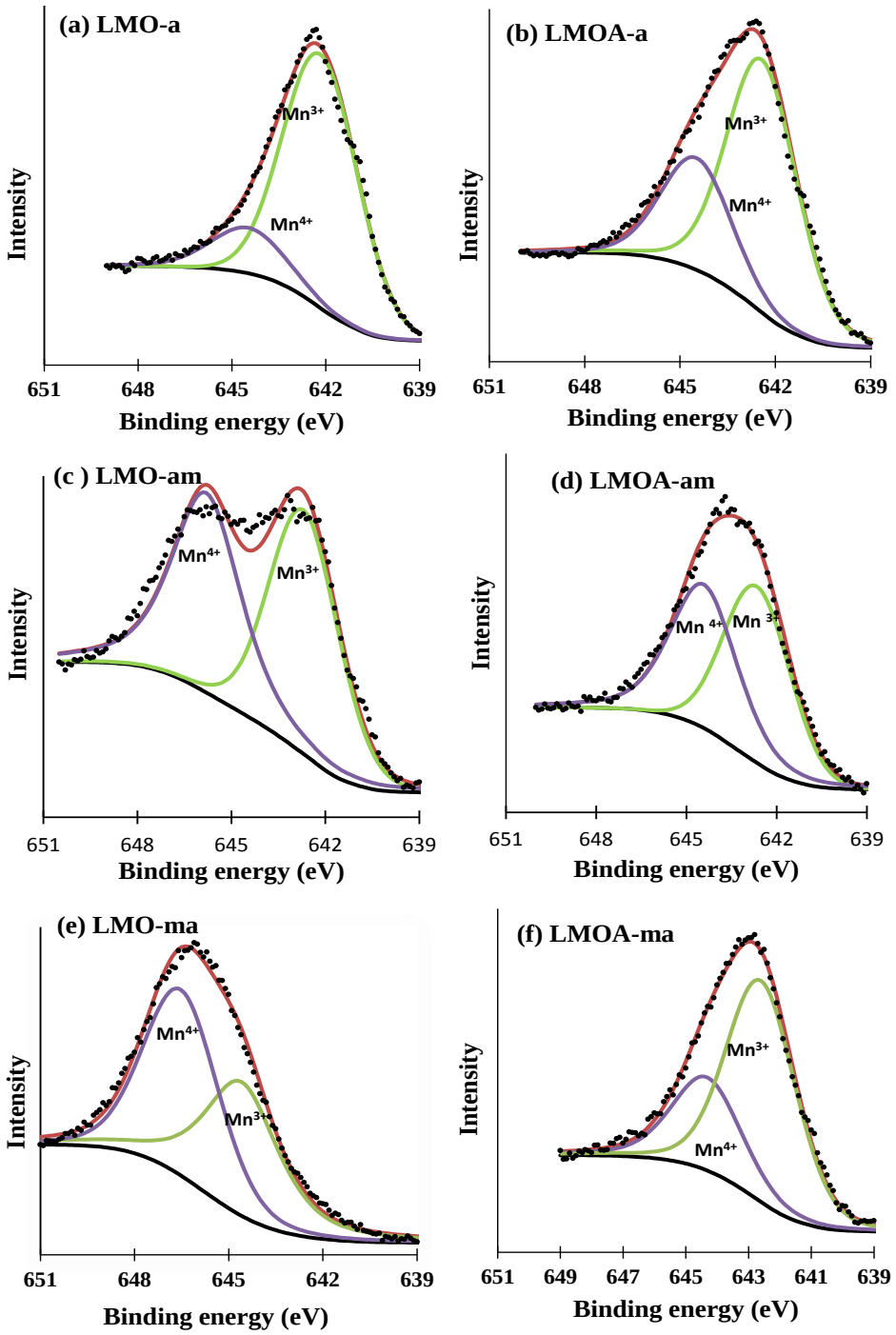

Fig. 5: XPS Mn $2p_{3/2}$ spectra of LMO- and LMOA-based samples.

The electrochemistry of the coin cells was studied as shown in **Fig. 6**. The cyclic voltammetric evolutions of the LMO and LMOA-based coin cells (**Fig. 6a,b**) showed two redox couples (I/I' and II/II'), indicating an expected two-step lithium ion insertion/extraction reactions.[45] The shoulder peak *ca.* 3.874 V (peak III) of the LMO-ma is attributed to the

'formation cycle' during initial cycles whereby minor structural rearrangement of the lattice takes occur.[46] From the CV data (summarised in *Supporting Information*, ***Table S1***) clearly indicate reversibility of the redox processes, with the microwave-treated samples showing enhanced reaction kinetics compared to the un-microwaved samples. The discharge capacities **(Fig. 6c,d**) for the LMOA based coin cells are lower than that of un-doped LMO sample due to the replacement of the redox-active Mn^{3+} with redox-inactive Al^{3+} in the spinel structure. From the rate capability studies (**Fig. 6e,f)** the microwave-treated samples (LMO-am, LMOA-am and LMOA-ma) gave higher capacities at high C-rates and showed almost the same capacity when returned to the initial 0.1 C-rate compared to the standard LMO and LMOA-based coin cells.

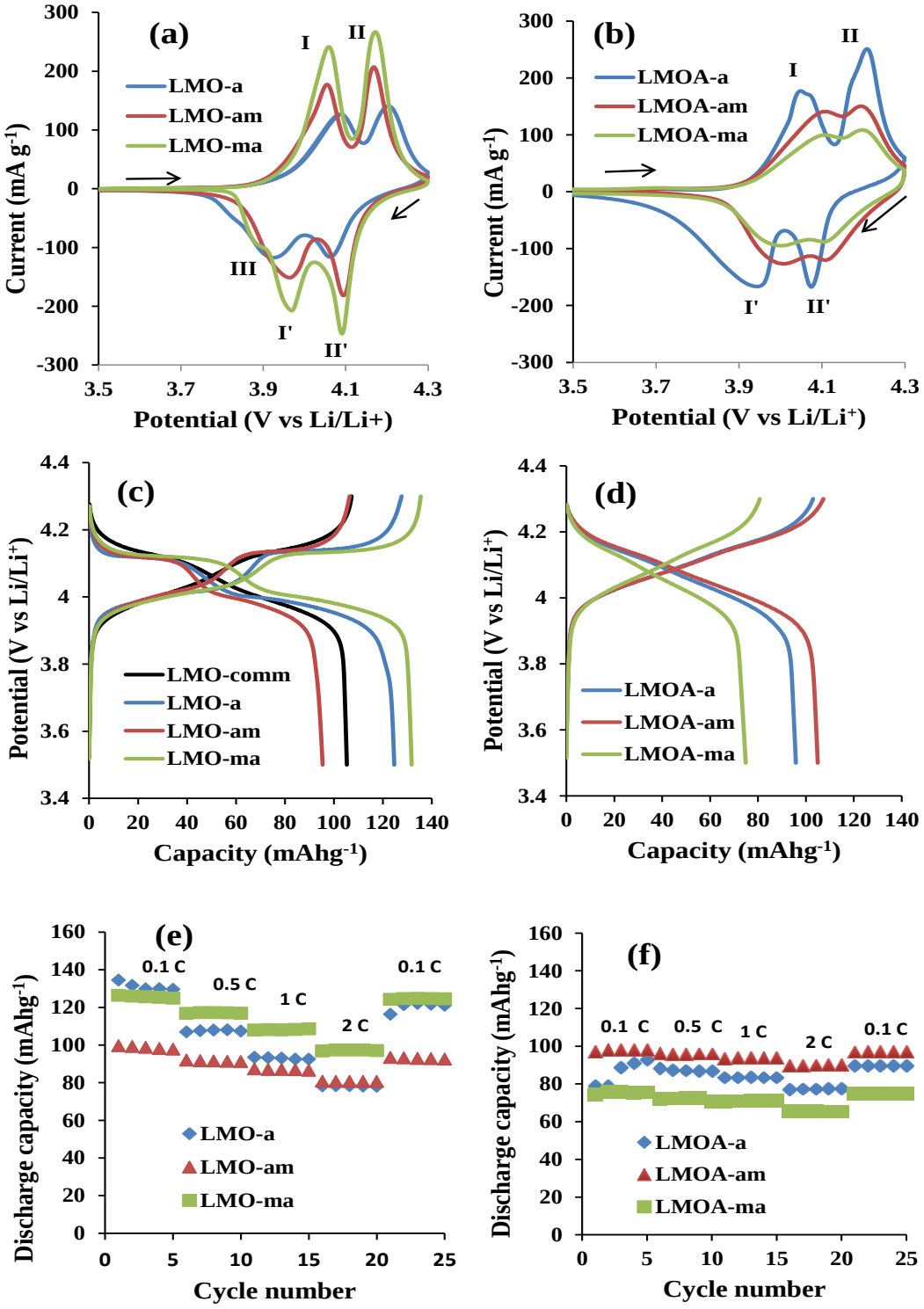

Fig. 6: Cyclic voltammograms of LMO (a) and LMOA (b) coin cells at 0.1 mVs^{-1}; Galvanostatic charge-discharge of LMO (c) and LMOA (d) coin cells at 0.1 C; Plots of discharge capacity vs cycle number for the LMO (e) and LMOA (f) coin cells at different current densities (0.1 – 2 C) between 3.5 – 4.3 V range.

There are critical findings from the coin cell data in **Table 1** (also from discharge capacity vs. cycle number vs. coulombic efficiency curves in *Supporting Information,* ***Fig. S5***) that should be emphasised. First, the LMO obtained by a short microwave exposure prior to annealing (i.e., LMO-ma materials with $n_{Mn} \approx 3.5+$) gave the highest initial capacity (131.5 $mAhg^{-1}$) and best capacity retention (95% even after 50 cycles). These results were shown to be similar to LMO obtained from microwave-assisted synthesis [44] (also with $n_{Mn} \approx 3.5+$) that gave poor performance (initial capacity of 118.6 $mAhg^{-1}$, and 33.2% capacity retention after 50 cycles). Thus, the high-performance of our LMO-ma stems solely from our strategic microwave synthesis protocol. Second, the best-performing LMO and LMOA are those with $n_{Mn} \approx 3.5+$ which were obtained by a pre- or post-annealing microwave irradiation step. Third, all the LMOA samples showed lower discharge capacity but, interestingly, gave excellent capacity retention, the microwaved samples giving the highest performance. Fourth, LMO-a (with $n_{Mn} = 3.165+$, capacity retention of 88%) can be optimized or tuned to give $n_{Mn} = 3.5+$ and thus enhanced capacity retention (91%) by subjecting the powder to microwave irradiation. The same phenomenon is also observed for the LMOA-a (with $n_{Mn} = 3.310+$, capacity retention of 92.8%) which gave $n_{Mn} = 3.5$ with enhanced capacity and capacity retention (99.6%). Finally, LMOA-a and LMOA-ma with lower average manganese oxidation state ($n_{Mn} \approx 3.31+$) gave better capacity retention than LMO-am and LMO-ma with higher n_{Mn} values of *ca.* 3.50+ and 3.54+, respectively. Our results largely contradict various reports that predicted that higher capacity retention could be obtained only at $n_{Mn} > 3.50+$.[14, 15, 47, 48] Also, Zhang *et al.* [19] reported that the best performing dual-doped LMO was with $n_{Mn}= 3.571+$. We can infer from our findings that LMO and doped-LMO with $n_{Mn} \approx 3.5+$ with excellent capacity retention can be obtained if microwave irradiation is strategically used in the synthesis step, pre or post-annealing steps. The order of the effect of MWI is not the same for the LMO and LMOA materials because the LMO sample is a different material from

LMOA sample because the Al doping in LMOA changed the chemistry, especially the electrochemistry of LMO. This is evident from the lower capacities obtained for LMOA compared to LMO.

Conclusions

Previously, the average valence (n_{Mn}) of manganese has been known to be the determining factor for capacity retention in $LiMn_2O_4$ and doped-$LiMn_2O_4$ spinel cathode materials for rechargeable lithium ion battery. When the concentration of Mn^{3+} ions exceeds that of Mn^{4+} ions ($n_{Mn} < 3.5+$) capacity fade/loss becomes prominent, but when $n_{Mn} > 3.5+$ capacity retention is improved. We report, for the first time, the application of microwave irradiation to optimise the manganese valence states in $LiMn_2O_4$ and Al doped-$LiMn_2O_4$ for enhanced capacity retention. We showed that this strategic microwave irradiation can be used to simultaneously shrink the spinel particles and lattice parameters for improved crystallinity, and tune the Mn^{3+}/Mn^{4+} ratio to obtain $n_{Mn} \approx 3.5+$ for enhanced electrochemical performance. Thus, the electrochemistry of LMO and LMOA can be enhanced by tuning the manganese valence to *ca.* 3.5+ by strategic application of microwave irradiation in the pre- or post-annealing step. If microwave irradiation prior to annealing fails to achieve the $n_{Mn} \approx 3.5+$, one can still obtain the $n_{Mn} \approx 3.5+$ by microwave irradiation after annealing. Clearly, microwave irradiation cannot just be used as a mere heat source to achieve fast chemical reaction, but can be used to tune the physico-chemical properties of electrode materials. Thus, this study has the potential to revolutionize how we use microwave irradiation in the preparation of spinel materials and a plethora of materials for energy storage and conversion systems for enhanced performance. The process is being optimized at our laboratory for pilot-scale production.

Acknowledgements

We thank the CSIR and the NRF for supporting this work. FPN thanks the CSIR for studentship.

References

1 B. Scrosati, *Electrochim. Acta*, 2000, **45**, 2461-2466.

2 T. Ohzuku and R. J. Brodd, *J. Power Sources*, 2007, **174**, 449-456.

3 J. Amarilla, K. Petrov, F. Pico, G. Avdeev, J. Rojo and R. Rojas, *J. Power Sources*, 2009, **191**, 591-600.

4 B. Dunn, H. Kamath and J. M. Tarascon, *Science*, 2011, **334**, 928-935.

5 J. Tarascon and M. Armand, *Nature*, 2001, **414**, 359-367.

6 M. Armand and J. Tarascon, *Nature*, 2008, **451**, 652-657.

7 G. Amatucci and J. Tarascon, *J. Electrochem. Soc.*, 2002, **149**, K31-K46.

8 K. Kang, Y. S. Meng, J. Breger, C. P. Grey and G. Ceder, *Science*, 2006, **311**, 977-980.

9 P. Ragupathy, *RSC Advances*, 2014, **4**, 670-675.

10 N. Choi, Z. Chen, S. A. Freunberger, X. Ji, Y. Sun, K. Amine, G. Yushin, L. F. Nazar, J. Cho and P. G. Bruce, *Angewandte Chemie International Edition*, 2012, **51**, 9994-10024.

11 S. Lee, Y. Cho, H. Song, K. T. Lee and J. Cho, *Angewandte Chemie International Edition*, 2012, **51**, 8748-8752.

12 M. M. Thackeray, Y. Shao-Horn, A. J. Kahaian, K. D. Kepler, E. Skinner, J. T. Vaughey and S. A. Hackney, *Electrochemical and Solid-State Letters*, 1998, **1**, 7-9.

13 M. Qian, J. Huang, S. Han and X. Cai, *Electrochim. Acta*, 2014, **120**, 16-22.

14 S. Martinez, I. Sobrados, D. Tonti, J. Amarilla and J. Sanz, *Physical Chemistry Chemical Physics*, 2014, **16**, 3282-3291.

15 Q. Tong, Y. Yang, J. Shi, J. Yan and L. Zheng, *J. Electrochem. Soc.*, 2007, **154**, A656-A667.

16 R. Gummow, A. De Kock and M. Thackeray, *Solid State Ionics*, 1994, **69**, 59-67.

17 M. Reddy, M. S. Raju, N. Sharma, P. Quan, S. H. Nowshad, H. Emmanuel, V. Peterson and B. Chowdari, *J. Electrochem. Soc.*, 2011, **158**, A1231-A1236.

18 F. Jiao, J. Bao, A. H. Hill and P. G. Bruce, *Angewandte Chemie International Edition*, 2008, **47**, 9711-9716.

19 Y. Shin and A. Manthiram, *Chemistry of materials*, 2003, **15**, 2954-2961.

20 W. Choi and A. Manthiram, *J. Electrochem. Soc.*, 2007, **154**, A614-A618.

21 M. A. Kebede, M. J. Phasha, N. Kunjuzwa, L. J. Le Roux, D. Mkhonto, K. I. Ozoemena and M. K. Mathe, 2014, .

22 M. Nakayama, K. Watanabe, H. Ikuta, Y. Uchimoto and M. Wakihara, *Solid State Ionics*, 2003, **164**, 35-42.

23 H. Yan, X. Huang and L. Chen, *J. Power Sources*, 1999, **81–82**, 647-650.

24 S. Bao, Y. Liang and H. Li, *Mater Lett*, 2005, **59**, 3761-3765.

25 P. Ragupathy, H. N. Vasan and N. Munichandraiah, *Mater. Chem. Phys.*, 2010, **124**, 870-875.

26 Y. Fu, C. Lin, Y. Su, J. Jean and S. Wu, *Ceram. Int.*, 2004, **30**, 1953-1959.

27 B. He, W. Zhou, S. Bao, Y. Liang and H. Li, *Electrochim. Acta*, 2007, **52**, 3286-3293.

28 H. Liu, C. Hu, X. Zhu, H. Hao, J. Luo, J. Zhou and S. Ouyang, *Mater. Chem. Phys.*, 2004, **88**, 290-294.

29 Y. Sun, *Solid State Ionics*, 1997, **100**, 115-125.

30 X. M. Wu, X. H. Li, Z. B. Xiao, J. Liu, W. B. Yan and M. Y. Ma, *Mater. Chem. Phys.*, 2004, **84**, 182-186.

31 X. Zhang, H. Zheng, V. Battaglia and R. L. Axelbaum, *J. Power Sources*, 2011, **196**, 3640-3645.

32 S. Bao, Y. Liang, W. Zhou, B. He and H. Li, *J. Power Sources*, 2006, **154**, 239-245.

33 T. Yi, C. Hao, C. Yue, R. Zhu and J. Shu, *Synth. Met.*, 2009, **159**, 1255-1260.

34 H. Zhang, D. Liu, X. Zhang, C. Zhao and Y. Xu, *Journal of Solid State Electrochemistry*, 2014, **18**, 569-575.

35 H. Zhang, Y. Xu, D. Liu, X. Zhang and C. Zhao, *Electrochim. Acta*, 2014, .

36 S. H. Chang, K. S. Ryu, K. M. Kim, M. S. Kim, I. K. Kim and S. G. Kang, *J. Power Sources*, 1999, **84**, 134-137.

37 H. Chen and D. Hsu, *J. Alloys Compounds,* 2014, **598**, 23-26.

38 H. Chen and D. Hsu, *Appl. Surf. Sci.*, 2014, **290**, 161-166.

39 E. Elbadraoui, J. Baudour, F. Bouree, B. Gillot, S. Fritsch and A. Rousset, *Solid State Ionics,* 1997, **93**, 219-225.

40 C. J. Jafta, M. K. Mathe, N. Manyala, W. D. Roos and K. I. Ozoemena, *ACS applied materials & interfaces,* 2013, **5**, 7592-7598.

41 J. F. Marco, J. R. Gancedo, M. Gracia, J. L. Gautier, E. I. Ríos, H. M. Palmer, C. Greaves and F. J. Berry, *Journal of Materials Chemistry,* 2001, **11**, 3087-3093.

42 V. Mittal, P. Chandramohan, S. Bera, M. Srinivasan, S. Velmurugan and S. Narasimhan, *Solid State Commun.*, 2006, **137**, 6-10.

43 J. Töpfer, A. Feltz, D. Gräf, B. Hackl, L. Raupach and P. Weissbrodt, *physica status solidi (a),* 1992, **134**, 405-415.

44 T. Yamashita and P. Hayes, *Appl. Surf. Sci.,* 2008, **254**, 2441-2449.

45 M. Reddy, A. Sakunthala, S. SelvashekaraPandian and B. Chowdari, *The Journal of Physical Chemistry C,* 2013, **117**, 9056-9064.

46 X. Zhao, M. Reddy, H. Liu, S. Ramakrishna, G. S. Rao and B. Chowdari, *RSC Advances,* 2012, **2**, 7462-7469.

47 Y. Shin and A. Manthiram, *J. Electrochem. Soc.*, 2004, **151**, A204-A208.

48 R. J. Gummow, A. de Kock and M. M. Thackeray, *Solid State Ionics,* 1994, **69**, 59-67

SUPPORTING INFORMATION

Microwave-assisted optimization of the manganese redox states for enhanced capacity and capacity retention of $LiAl_xMn_{2-x}O_4$ (x = 0 and 0.3) spinel materials

Funeka P. Nkosi[1,2], Charl J. Jafta[2], Mesfin Kebede[2], Lukas le Roux[2], Mkhulu K. Mathe[2] and Kenneth I. Ozoemena[*,1,2]

[1.] *Department of Chemistry, University of Pretoria, Pretoria 0002, South Africa.*

[2.] *Energy Materials, Materials Science and Manufacturing, Council for Scientific & Industrial Research (CSIR), Pretoria 0001, South Africa*

A manuscript to be submitted to *RSC Advances*

[*]Author to whom correspondence should be addressed: (K.I. Ozoemena): Tel.:+27128413664; Fax: +27128412135; E-mail: kozoemena@csir.co.za

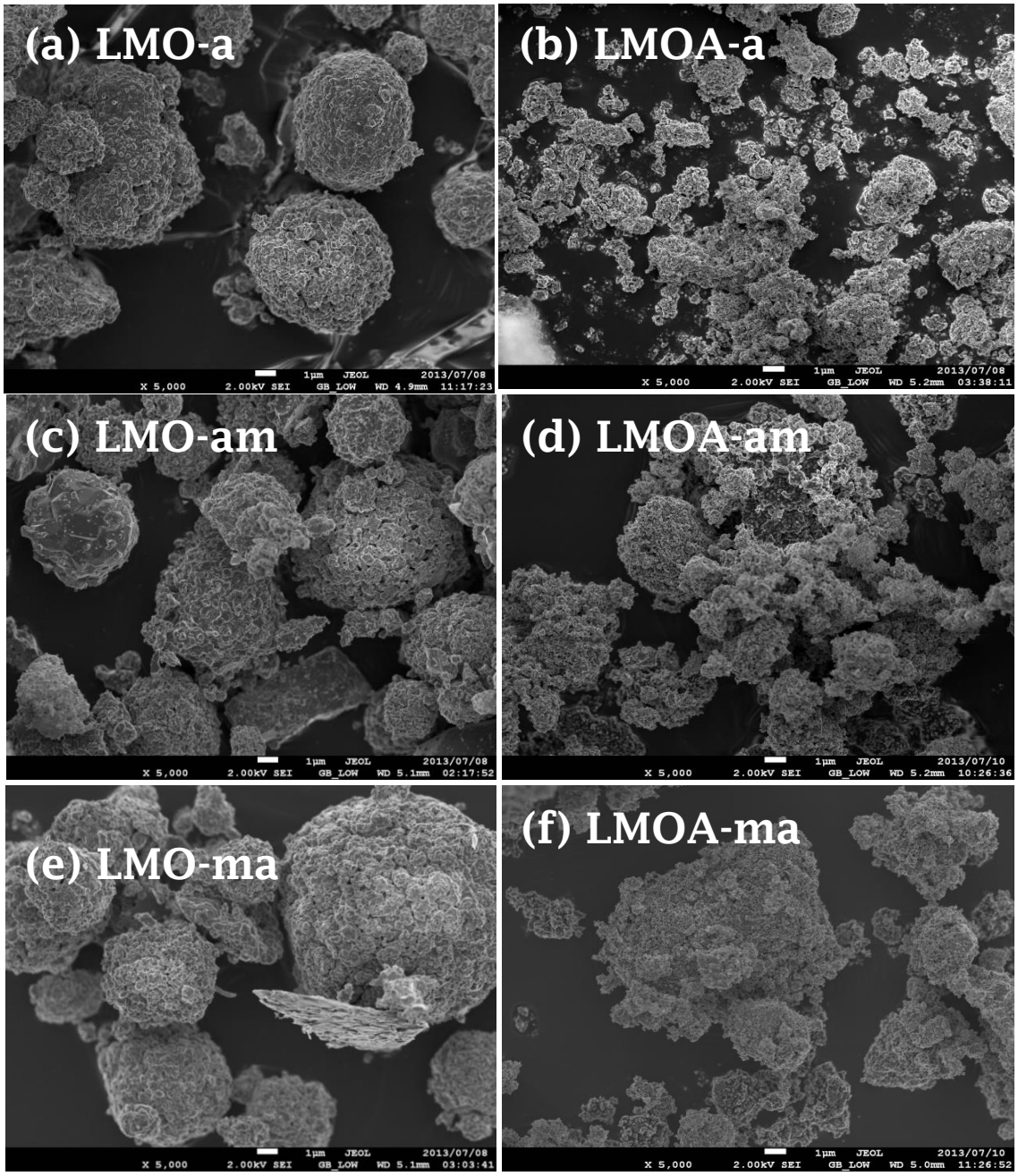

Fig. S1: Typical SEM images of $LiMn_2O_4$ (LMO) and $LiAl_{0.3}Mn_{1.7}O_4$ (LMOA) powders at high magnifications (1 μm). The abbreviations are as described in the main text; where symbols "**a**" means the materials was obtained by conventional high-temperature annealing process; "**am**" means that the material was subjected to microwave irradiation after obtaining the powder by high-temperature annealing; and "**ma**" means the material was subjected to microwave irradiation prior to annealing.

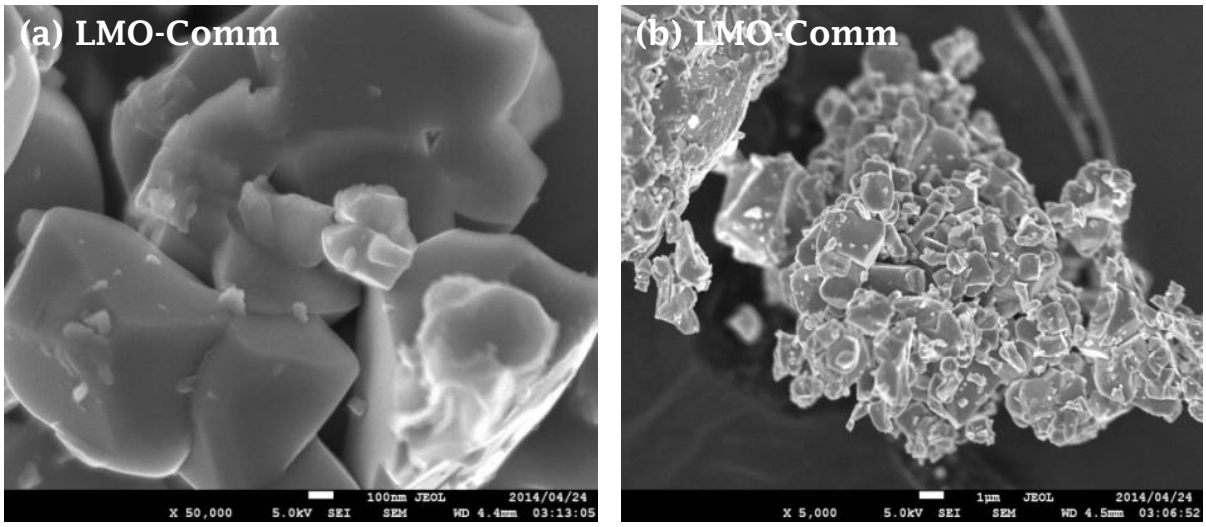

Fig. S2: SEM images of the standard commercial LMO material (LMO-comm, CAS No.: 39457-42-6, MTI Corporation, Richmond, CA., USA)

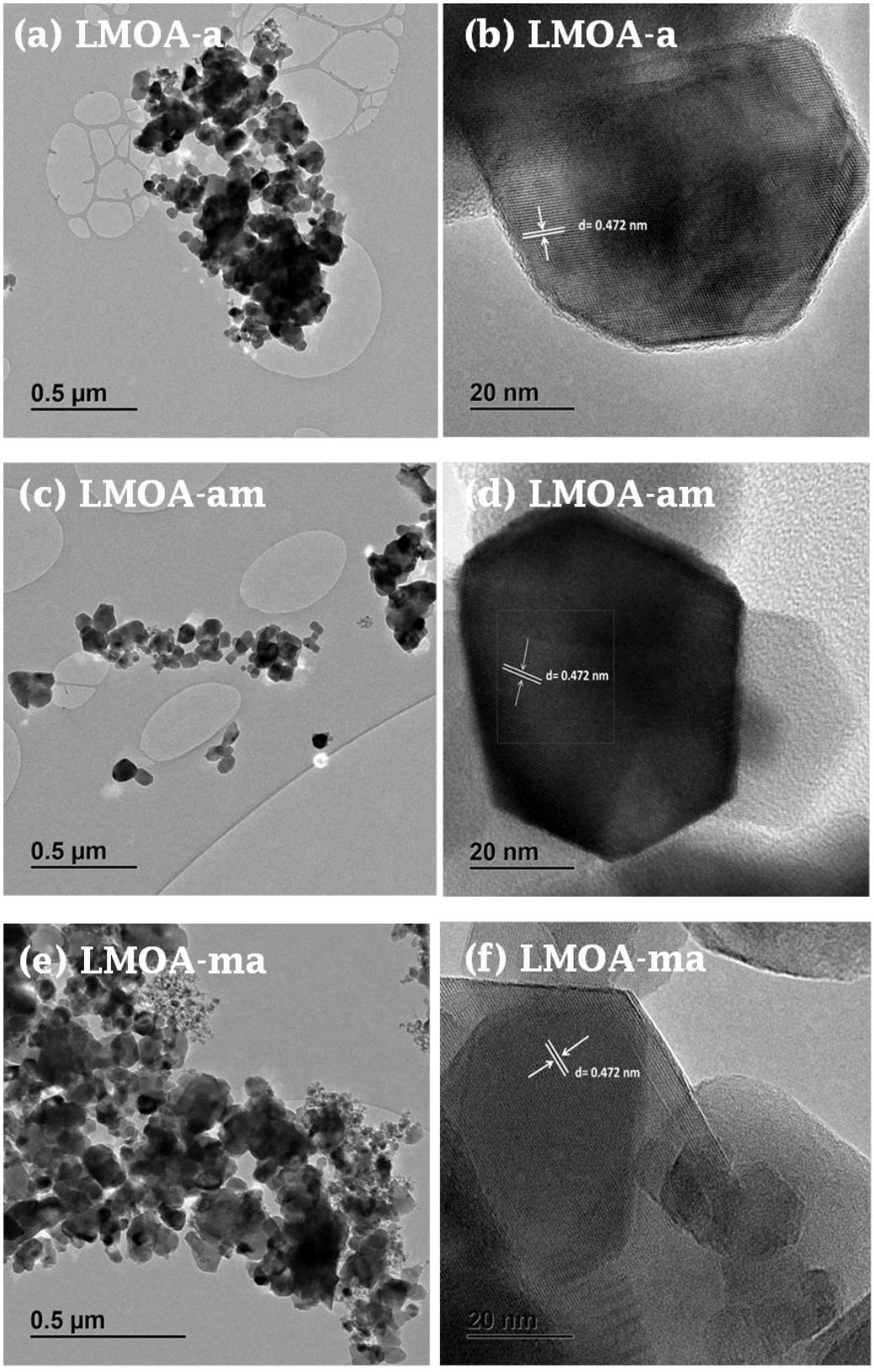

Fig. S3: Typical TEM and HRTEM images of LMOA-based powders. The abbreviations are the same as described in the main text and in ***Figure S1***.

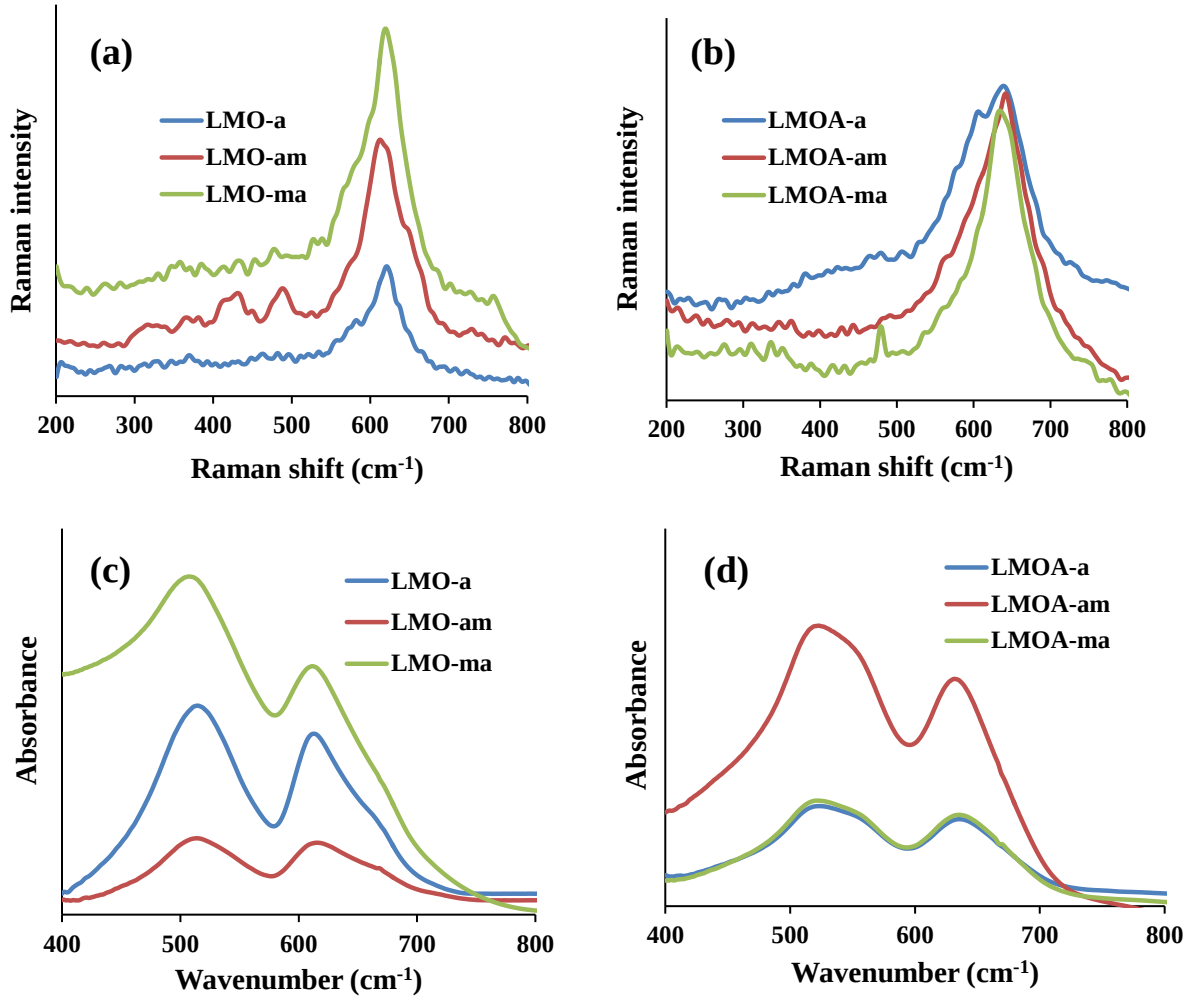

Fig. S4: Raman (a, b) and IR (c, d) spectra of the LMO- and LMOA-based spinels.

The Raman and IR spectral data (*Supporting Information,* ***Figure S4***) are consistent with literature for LMO based spinels.[1] From the Raman spectra, the LMO samples showed pronounced peaks around 625 cm^{-1} while the LMOA samples showed a positive shifts in the 632 – 642 cm^{-1} range. The peaks around the 600 – 650 cm^{-1} are due to the symmetric Mn-O stretching vibration of the MnO_6 groups, assigned to the A_{1g} species in the O_h^7 spectroscopic space group. [2] The broadening of these peaks can be attributed to the cation-anion bond lengths and polyhedral distortion occurring in LMO (i.e., the stretching vibrations of $Mn^{3+}O_6$

and $Mn^{4+}O_6$ octahedra). The positive shift of the peaks for the LMOA-based peak samples compared to the un-doped LMO is due to the existence of Al^{3+} ions in some of the octahedral sites. Mn^{4+} has a large spin orbital constant of *ca*. 138 cm^{-1} compared to Mn^{3+} with spin orbital splitting of *ca*. 90 cm^{-1}, thus the bond strength of Mn^{4+}-O increases after doping with Al^{3+} ions and thus result in the peak shifts. On the other hand, the IR spectra of the samples were dominated by two intense absorption bands in the finger print regions due the presence of the F_{1u} species, with the high frequency bands ($\geq$ 600 cm^{-1}) relating to the asymmetric stretching modes of MnO_6 group. The bands appeared at *ca.* 613/515, 616/514 and 612/507 cm^{-1} for LMO-A, LMO-AM and LMO-MA, respectively, and at higher wavenumbers of *ca.* 635/523, 632/523, and 635/522 cm^{-1} for LMOA-A, LMOA-AM and LMOA-MA, respectively. The LMOA samples showed positive shift in the peak positions ($\geq$ 20 cm^{-1}) positive shift in the peaks for the LMOA-based spinels is related to the which indicates a relatively stronger bonding in the $Mn(Al)O_6$ octahedra due to Al-doping and the microwave irradiation. The Al-O bond (512 $kJmol^{-1}$) is stronger than the Mn-O bond (402 kJ mol^{-1}) in the octahedron. Interestingly, it was the microwave-treated samples with $n_{Mn} \approx 3.5+$ (i.e., LMO-ma and LMOA-am) that gave the strongest Raman and IR peaks, clearly confirming the effect of the microwave irradiation in strengthening the Mn-O bonding for enhanced electrochemistry.

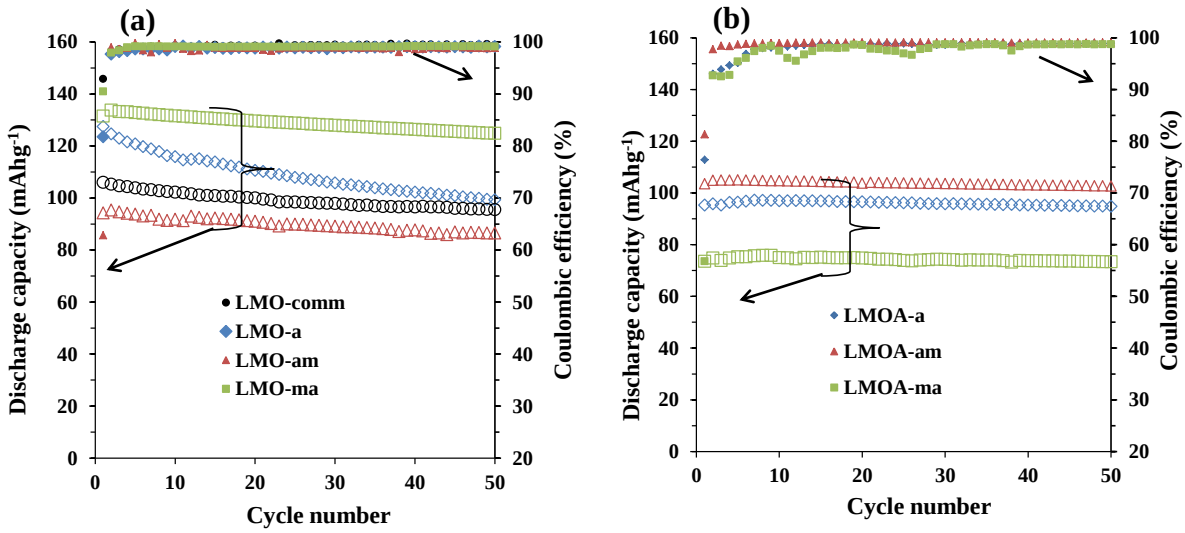

Fig. S5: Typical plots of discharge capacity vs cycle number vs coulombic efficiency for (a) LMO and (b) LMOA-based coin cell batteries.

Table S1: Cyclic voltammetric data for the redox couples shown by the LMO and LMOA-based coin cell batteries.

Material	I_{pa}/I_{pc}		ΔE_p **(V)**		$\Delta E_{1/2}$ **(V)**	
	Redox couple 1/1’	Redox couple 2/2’	Redox couple 1/1’	Redox couple 2/2’	Redox couple 1/1’	Redox couple 2/2’
LMO-a	1.06	**1.22**	0.16	**0.12**	4.00	4.13
LMO-am	1.17	1.14	0.09	0.07	4.01	4.13
LMO-ma	1.18	1.09	0.08	0.07	4.01	4.13
LMOA-a	1.07	**1.50**	0.10	**0.13**	4.00	4.14
LMOA-am	1.12	1.22	0.11	0.08	4.05	4.15
LMOA-ma	1.05	1.25	0.10	0.09	4.05	4.15

References

1 A. Paolone, A. Sacchetti, T. Corridoni, P. Postorino, R. Cantelli, G. Rousse and C. Masquelier, *Solid State Ionics* 2004, **170**, 135-138.

2 C.M. Julien and M. Massot, *Materials Science and Engineering: B* 2003, **97**, 217-230.